Comparison of Nimbus-7 SMMR and GOES-1 VISSR Atmospheric Liquid Water Content

JEAN-YVES LOJOU

Centre de Recherches en Physique de l'Environnement, Issy-les-Moulineaux, France

ROBERT FROUIN

California Space Institute, Scripps Institution of Oceanography, La Jolla, California

RENÉ BERNARD

Centre de Recherches en Physique de l'Environnement, Issy-les-Moulineaux, France

(Manuscript received 11 October 1989, in final form 22 July 1990)

ABSTRACT

Vertically integrated atmospheric liquid water content derived from Nimbus-7 Scanning Multichannel Microwave Radiometer (SMMR) brightness temperatures and from GOES-1 Visible and Infrared Spin-Scan Radiometer (VISSR) radiances in the visible are compared over the Indian Ocean during MONEX (monsoon experiment). In the retrieval procedure, Wilheit and Chang's algorithm and Stephens' parameterization schemes are applied to the SMMR and VISSR data, respectively. The results indicate that in the 0–100 mg cm^{-2} range of liquid water content considered, the correlation coefficient between the two types of estimates is 0.83 (0.81–0.85 at the 99 percent confidence level). The Wilheit and Chang algorithm, however, yields values lower than those obtained with Stephens's schemes by 24.5 mg cm^{-2} on the average, and occasionally the SMMR-based values are negative. Alternative algorithms are proposed for use with SMMR data, which eliminate the bias, augment the correlation coefficient, and reduce the rms difference. These algorithms include using the Wilheit and Chang formula with modified coefficients (multilinear regression), the Wilheit and Chang formula with the same coefficients but different equivalent atmospheric temperatures for each channel (temperature bias adjustment), and a second-order polynomial in brightness temperatures at 18, 21, and 37 GHz (polynomial development). When applied to a dataset excluded from the regression dataset, the multilinear regression algorithm provides the best results, namely a 0.91 correlation coefficient, a 5.2 mg cm^{-2} rms (residual) difference, and a -2.9 mg cm^{-2} bias. Simply shifting the liquid water content predicted by the Wilheit and Chang algorithm does not yield as good comparison statistics, indicating that the occasional negative values are not due only to a bias. The more accurate SMMR-derived liquid water content allows one to better evaluate cloud transmittance in the solar spectrum, at least in the area and during the period analyzed. Combining this cloud transmittance with a clear sky model would provide ocean surface insolation estimates from SMMR data alone.

1. Introduction

The advantage of exploiting satellite-based passive microwave measurements to observe ocean surface parameters, such as sea surface temperature and wind speed, resides in their ability to remain sensitive to the parameters even in cloudy conditions. In addition to sensing surface parameters, passive microwave measurements can also be employed to remotely sense vital climatological variables, most notably atmospheric water vapor and liquid water contents. The characterization of cloud water content is particularly important in water budget assessments and radiative transfer modeling.

In 1979 Wilheit and Chang proposed a basic regression algorithm to compute cloud liquid water content from NIMBUS-7 Scanning Multichannel Microwave Radiometer (SMMR) brightness temperatures. The algorithm, established from a synthetic dataset and theoretical calculations, employs the dually polarized 18, 21, and 37 GHz SMMR channels. Uncertainties in the modeling and the lack of verification, however, have limited the application of the Wilheit and Chang algorithm. In some instances, the algorithm was shown to produce negative values which, ". . . are probably due to only one bias," (Katsaros and Lewis 1986).

Although less sensitive to liquid water, the other SMMR channels, which measure at 6.6 and 10.7 GHz, have also been used by Prabhakara et al. (1983) to

Corresponding author address: Dr. Robert Frouin, California Space Inst., Mail Code A-021, Scripps Inst. of Oceanography, La Jolla, CA 92093.

retrieve atmospheric liquid water content. In that case, the difference between the deviations of the 6.6 and 10.7 GHz brightness temperatures from their values when the sea surface is calm and the sky is clear (assumed to correspond to the minimum brightness temperature at 6.6 GHz during a month at a given geographic location), correlates with the amount of liquid water in the atmosphere. The problem with this approach, as pointed out by Prabhakara et al., is that the deviations indicate the effect of either surface roughness or liquid water, and it is not always possible to distinguish between the two types of influence. Another disadvantage is that at 6.6 GHz the SMMR spatial resolution is degraded to 155 km (compared to 30 km at 37 GHz).

In this context, it appears necessary to compare liquid water contents estimated using the aforementioned algorithms with those obtained independently or measured. So far, such comparisons have been only qualitative in nature (e.g., Taylor et al. 1983). In situ measurements are difficult to make and the resulting dataset is likely to be insufficient for statistical significance.

An alternative method of producing independent liquid water content estimates is to combine satellite techniques to retrieve cloud reflectance in the visible (e.g., Gautier et al. 1980) with validated theoretical relations between cloud reflectance and liquid water path (Stephens 1978b; Stephens et al. 1984).

This approach is selected in the present study. The liquid water content obtained from cloud reflectance in the visible is compared with corresponding SMMR estimates. Because of the limitations of the Prabhakara et al. technique, the SMMR estimates are derived only according to Wilheit and Chang. The data used in the comparison are GOES-1 VISSR radiances in the visible and concomitant NIMBUS-7 SMMR brightness temperatures acquired in June 1979 during MONEX.

After describing the retrieval schemes, data, and computational procedure, the comparison results are presented. Then, several modifications are proposed to the Wilheit and Chang algorithm which improve the comparison statistics. Validation of the modified liquid water content algorithms is accomplished using a dataset separate from the regression dataset. Finally, the usefulness of these algorithms for estimating surface insolation over the oceans is discussed.

2. Liquid water content retrieval

a. SMMR technique

In the microwave spectral region, where the Rayleigh–Jeans approximation holds, the radiative transfer in the atmosphere can be expressed simply as:

$$\frac{\partial T_B}{\partial z} = -\Gamma(T_B - T) \qquad (1)$$

where T_B and T are the brightness and thermodynamic temperatures at level z, respectively, and Γ is the absorption coefficient at level z. In this formulation, the propagation is along the z-axis.

If the absorption coefficient is sufficiently small, (1) can be integrated easily by horizontally stratifying the atmosphere into a number of thermodynamically homogeneous layers. Each layer absorbs part of the incoming radiation and radiates according to its own thermodynamic temperature.

The radiation energy (or brightness temperature) measured by a microwave radiometer viewing the sea surface from above comes partly from the atmosphere itself, either directly or after reflection by the surface, and partly from the surface. Sky radiation after two-way absorption by the atmosphere and reflection by the surface also contributes to the signal. This contribution, or cosmic background, is always slight, except at viewing angles close to the direction of sun specular reflection, in which case the sun contribution may be taken into account.

The signal measured by the radiometer can be easily modeled knowing the absorption properties of the atmospheric constituents and the surface emissivity. Unlike the atmospheric contribution, the radiation energy reflected and emitted by the surface is strongly polarized.

The atmosphere is then divided into N layers of arbitrary thickness. If Γ_j denotes the absorption coefficient of layer j, the brightness temperature measured by the radiometer at satellite altitude can be written as (Millet 1984):

$$T_B = \sum_{j=1}^{N} T_j(1 - \Gamma_j)\gamma_{j+1}^{u} + \epsilon\gamma T_s + (1 - \epsilon)\gamma\Big[\sum_{j=1}^{N} T_j(1 - \Gamma_j)\gamma_{j-1}^{d} + \gamma T_{\text{sky}}\Big] \qquad (2)$$

where γ_j^u is the total absorption coefficient for upwelling radiation from layer j (characterizes the absorption of the $N - j$ layers above layer $j - 1$: $\gamma_j^u = \prod_{k=j}^{N} \Gamma_k$), γ_j^d is the absorption coefficient for downwelling radiation from layer j (characterizes the absorption of the j first layers above the sea surface: $\gamma_j^d = \prod_{k=1}^{j} \Gamma_k$), γ is the total absorption coefficient for the entire atmosphere ($\gamma = \gamma_1^u = \gamma_N^d$), T_j is the temperature of layer j, T_{sky} is the sky equivalent radiative temperature (including the cosmic residual and galactic contribution), and ϵ is the surface emissivity.

Using this kind of modeling and a synthetic database of atmospheric profiles and surface parameters, Wilheit and Chang developed a formalism to retrieve sea surface temperature, wind speed near the sea surface, and vertically integrated atmospheric water vapor and liquid water contents from a linear combination of brightness temperatures in the NIMBUS-7 SMMR channels. Because of the approximate logarithmic relation between brightness temperature and atmospheric optical thickness, Wilheit and Chang used the variable:

$$X = \log_e(T_e - T_B) \quad (3)$$

where T_e is the equivalent temperature of the atmosphere (T_e = 280 K).

For liquid water content, the algorithm reads:

$$\begin{aligned} LW = {} & 246.1 - 3.391\theta \\ & + 134.40 \log_e(280. - T_b^{18H}) \\ & - 51.72 \log_e(280. - T_B^{18V}) \\ & + 24.95 \log_e(280. - T_B^{21H}) \\ & + 46.14 \log_e(280. - T_B^{21V}) \\ & - 36.63 \log_e(280. - T_B^{37H}) \\ & - 155.50 \log_e(280. - T_B^{37V}) \end{aligned} \quad (4)$$

where LW is liquid water content in mg cm^{-2} and θ is the viewing angle in degrees. The present study intends to test the validity of (4).

b. *VISSR technique*

Cloud albedo in the solar spectrum is strongly related to liquid water content varies little although significantly with drop-size distribution and is practically independent of liquid water vertical distribution (e.g., Sephens 1978a; Welch et al. 1980). This led Stephens (1978b) to parameterize cloud albedo as a function of only liquid water content for a fixed radiation geometry (solar zenith angle). Thus, using Stephens' (1978b) relationships with a cloud albedo measurement, which can be made from an earth-orbiting satellite, one can determine liquid water content.

For practical purposes it is assumed that the cloud albedo is measured at wavelengths in the visible portion of the solar spectrum. In this case, absorption by the cloud droplets is negligible. Further neglecting reflection by the sea surface, the albedo of a cloud layer of optical thickness τ_c can be approximated as (Coakley and Chýlek 1975):

$$A_c = \frac{\beta(\mu_0)\tau_c/\mu_0}{1 + \beta(\mu_0)\tau_c/\mu_0} \quad (5)$$

where μ_0 is the cosine of solar zenith angle and β the backscattered fraction of incident radiation (assumed monodirectional) at the cloud top. Using a detailed multiple-scattering model to calculate A_c for standard cloud types, Stephens (1978b) and Stephens et al. (1984) have tuned (5) to yield average values of β in the spectral range 0.3–0.75 μm. Stephens (1978b) also provided a least square-fit parameterization of the relationship between cloud optical thickness (determined from Mie theory for standard cloud types) and liquid water content:

$$\log_{10}\tau_c = 0.2633 + 1.7095 \log_e[\log_{10}\mathrm{LW}] \quad (6)$$

where LW is the liquid water content in $10 \times$ mg cm^{-2}.

Since this study is interested in obtaining LW from A_c, (5) is written as:

$$\beta(\mu_0)\tau_c = \mu_0 \frac{A_c}{1 - A_c}. \quad (7)$$

In this equation, $\beta\tau_c$ is a monotonous function of τ_c (see Fig. 1), which makes it possible to extract τ_c from A_c and, therefore, deduce LW from τ_c using (6).

Figure 2 displays LW as a function of A_c for various solar zenith angles. For LW > 100 mg cm^{-2}, A_c is almost insensitive to LW. This results from the functional form of A_c (A_c goes slowly to 1 as τ_c goes to infinity), and can be explained simply by considering that for thick clouds the backscattering contribution of the lower part of the cloud is small. In the cases studied later in this paper, the clouds are sufficiently thin to apply the above formalism confidently.

Stephens' (1978b) shortwave parameterization scheme has been verified for specific cases of planetary boundary layer clouds (Stephens et al. 1978). Predictions were in agreement with measurements within experimental uncertainties (about 15 percent). Other studies, in which aircraft observations of broadband solar irradiances were compared with theoretical calculations, have also concluded that measured cloud albedos are in satisfactory agreement with calculated values (e.g., Hignett 1987; Foot 1988). In these studies the radiative transfer calculations were performed with models similar to that used by Stephens (1978b) to derive his approximate formulas. The investigations, however, dealt with cloud albedo in the entire solar spectrum, which includes wavelengths (>0.75 μm) where droplet absorption is significant. More recently,

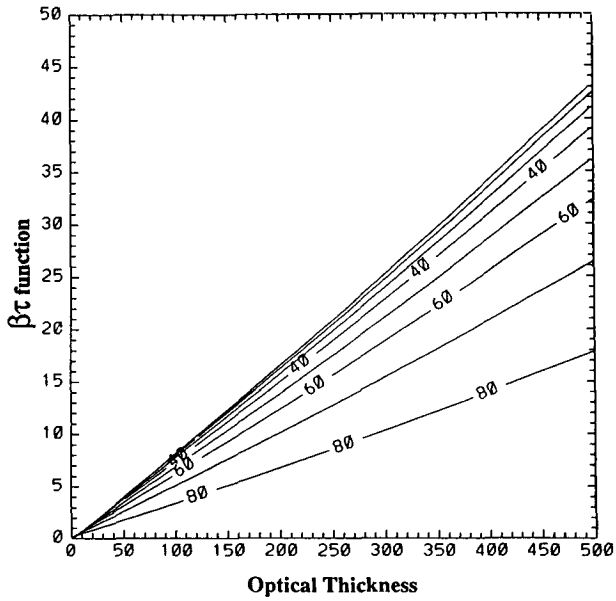

FIG. 1. Product of β and τ as a function of τ for various solar zenith angles.

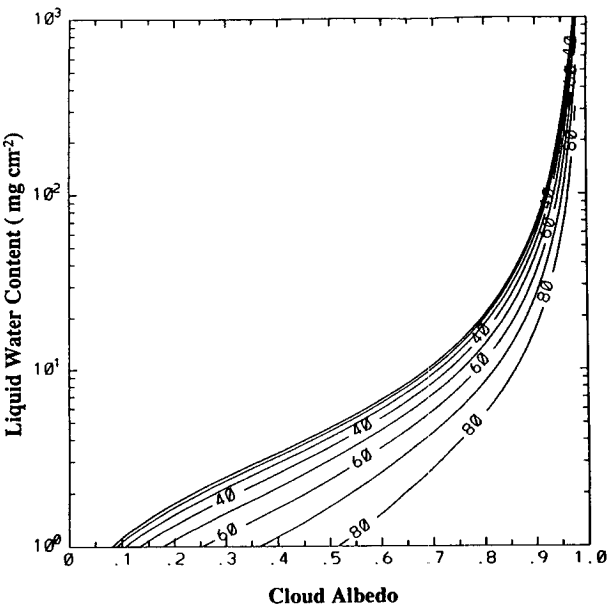

FIG. 2. Liquid water content, LW, as a function of cloud albedo, A_c, for various solar zenith angles.

Coakley and Snider (1988) compared cloud reflectivity obtained from the advanced very high resolution radiometer (AVHRR) 0.63 μm channel with cloud reflectivity calculated from Stephens' (1978b) formulas and liquid water content measured by an uplooking microwave radiometer installed on the ground. They found 20%–30% positive differences between parameterized and observed reflectivities which they could not explain. During the study period, however, the AVHRRs of the NOAA-9 and NOAA-10 satellites were experiencing a 15%–20% loss in sensitivity for the 0.63 μm channel (Whitlock et al. 1990: Teillet et al. 1988), which, thus, explains a large part of the discrepancy. Furthermore, as indicated by Coakley and Snider (1988), small-scale variability in the liquid water path may reduce the AVHRR cloud reflectivity and, thus, contribute to the observed bias.

In the present study cloud albedo is obtained from GOES VISSR radiance measured in the visible (0.5–0.75 μm channel) by solving the following equation (Diak and Gautier 1983):

$$\frac{\pi L_{\text{sat}}}{I_0 \cos\theta_0} = (1-a)(1-a') \times [\alpha + (1-\alpha)(1-\alpha') + A_c^2(1-\alpha)(1-\alpha')\alpha'] + (1-\alpha)(1-\alpha')(1-A_c)^2 A_s \quad (8)$$

where L_{sat} is the radiance measured at satellite altitude, I_0 is the extraterrestrial solar irradiance in the GOES VISSR solar channel, θ_0 is the sun zenith angle, a and a' are absorption coefficients for ozone of direct and diffuse solar radiation, respectively, α and α' are direct and diffuse reflection coefficients, respectively, and A_s is the surface albedo. It is assumed in (8) that the radiance reflected by the surface and clouds is isotropic. In actuality, bidirectional factors to convert radiances into irradiances may significantly depart from unity for some radiation geometries. In the cases considered later in the paper, however, θ_0 and θ remained within 30° and 50° of zenith, respectively, and for those angles ($\theta_0 < 30°$, $\theta < 50°$) the bidirectional effect is generally minimal (see for instance, Davis and Cox 1981; Taylor and Stowe 1984).

As mentioned above, subpixel variability because of the nonlinear relation between albedo and liquid water path may bias the VISSR liquid water content estimates. To examine this effect, this study follows Fairall et al. (1989) and expands cloud albedo about the average liquid water content in the VISSR pixel using a second-order Taylor approximation. The average liquid water in the pixel can then be expressed as:

$$\text{LW} = \text{LW}'\left[1 + S\left(\frac{\sigma}{\text{LW}}\right)^2\right] \quad (9)$$

where LW′ is the liquid water content deduced from the average cloud albedo in the VISSR pixel, σ is the standard deviation of liquid water content, and S is a nonlinear sensitivity coefficient defined as:

$$S = -\frac{1}{2}\left[\frac{\partial^2 A_c/\partial(\log_e \text{LW})^2}{\partial A_c/\partial(\log_e \text{LW})} - 1\right]. \quad (10)$$

Figure 3 shows S as a function of LW for various solar zenith angles. The sensitivity parameter is positive, varying from 0.1–0.8 in the liquid water range of interest. Fairall et al. (1989), using ground-based microwave measurements at San Nicholas Island during

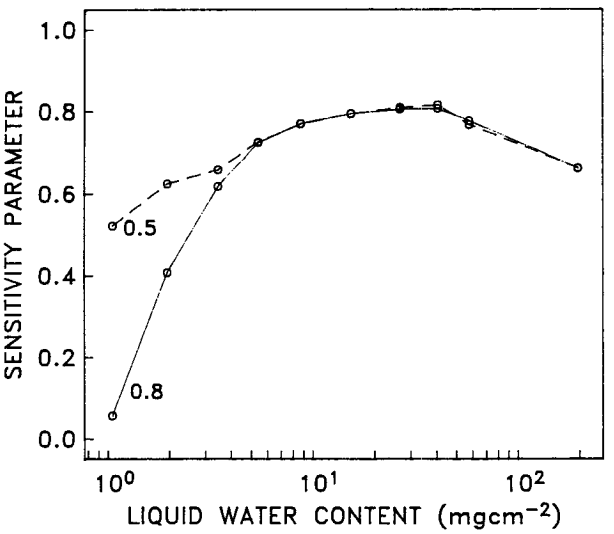

FIG. 3. Sensitivity parameter, S, as a function of liquid water content and cosine of solar zenith angle.

the First International Satellite Cloud Climatology Regional Experiment (FIRE) estimated $\sigma/LW = 0.25$ (a typical value) for stratocumulus clouds. This value, indeed, might not be valid for the clouds encountered during MONEX, but the objective here is to provide an order of magnitude for the subpixel variability effect. In the presence of small cumuli covering part of the filed of view, for instance, one would expect larger σ/LW values. Using $\sigma/LW = 0.25$ with $S = 0.8$, $LW = 1.05\ LW'$ is obtained, that is, liquid water content is underestimated by 5 percent only when neglecting subpixel variability.

3. Comparison between SMMR and VISSR liquid water content estimates

The comparison is made using NIMBUS-7 SMMR and GOES-1 VISSR data acquired over the Indian Ocean during MONEX. The date, time, and location of the satellite images selected are given in Table 1. Middle-level, convective clouds were generally present in the satellite images. These clouds are associated with the development of the southwest Indian monsoon (onset phase around 12 June 1979) and it is not excluded that some of the clouds may be precipitating. Except for 29 June 1979, the acquisition times for both types of data match closely. Although a maximum 59-minute difference exists between the SMMR and closest VISSR observations on 29 June 1979, the data are nonetheless utilized because of the particularly stable cloud field during that day. The comparison dataset corresponds not only to the smallest time differences between the VISSR and SMMR observations available, but also to minimum cirrus cloud contamination (checked visually) and average liquid water content in the SMMR pixels less than 100 mg cm^{-2} (estimated from the VISSR radiances).

The true SMMR brightness temperatures in the 18, 21, and 37 GHz channels (vertical and horizontal polarizations) were acquired from NASA in the cell-all tape format (Fu 1985). Since the spatial resolution of the instrument varies from about 30 km at 37 GHz to about 60 km at 18 GHz, the data remapped on the lower resolution (60 km) is extracted.

Prior to processing the data, the 21 GHz brightness temperatures is modified to account for a drift with time due to instrument malfunction. This was done by applying correction formulas suggested by Fu (1985). Note that this SMMR data were collected only eight months after the NIMBUS-7 launch; the corrections, therefore, were small.

The VISSR radiances in the visible channel were acquired from the Space Science and Engineering Center (SSEC) of the University of Wisconsin in the form of full resolution (about 1 km at nadir), 4 pixel-sampled, and uncalibrated brightness counts. The data was first converted into equivalent albedo assuming isotropy of the radiance field. This was done using calibration coefficients provided by Smith et al. (1981). Earth location was accomplished by using the SSEC navigation. This navigation was insufficiently accurate; for one image, in which landmarks were available along the coastline of Sri Lanka, the difference between computed and actual geographic locations was as much as 100 km. On the other hand, the only way to navigate the SMMR images was to use the orbitographic parameters.

In the comparison procedure, a translation was allowed between the SMMR and VISSR images due to the navigation uncertainties as well as time differences between the observations. The translation was determined by first computing a binary image for each type of measurement (thresholding the VISSR-derived cloud albedo remapped on the SMMR grid and the SMMR-derived liquid water content). The threshold was zero for both cloud albedo and liquid water content. SMMR pixels characterized by a negative liquid water content were assumed free of clouds. A displacement vector was then deduced from the best-lagged correlation (maximum of the cross-correlation product) between the binary images. In the next step, the liquid water content of VISSR pixels (about 225) included in the coarser resolution SMMR pixels translated was averaged as indicated above.

Since the VISSR data are 4 pixel-sampled, the effect of spatial sampling needs to be examined on the 60 $\times$ 60 km liquid water content estimates. This was done by comparing average estimates from nonsampled (all consecutive pixels) and 4 pixel-sample GOES-6 VISSR radiances acquired in June and July 1987 off the southern California coast. This dataset was used because a full resolution, nonsampled VISSR dataset was not available over the Indian Ocean during the season

TABLE 1. Date, time, and location of the satellite images used in the comparison.

Date	Latitude range	Longitude range	Acquisition time (GMT)	
			SMMR	VISSR
11 Jun 1979	08.1°S–06.4°N	59.8°E–70.0°E	07:31 to 07:36	0713 to 0718
17 Jun 1979	04.3°S–11.0°N	82.6°E–92.9°E	05:56 to 06:02	0612 to 0617
21 Jun 1979	02.5°S–12.2°N	63.4°E–73.6°E	07:12 to 07:17	0711 to 0716
23 Jun 1979	04.4°S–20.0°N	77.9°E–88.6°E	06:08 to 06:13	0609 to 0616
29 Jun 1979	06.4°S–9.2°N	79.8°E–89.0°E	06:13 to 06:18	0712 to 0717

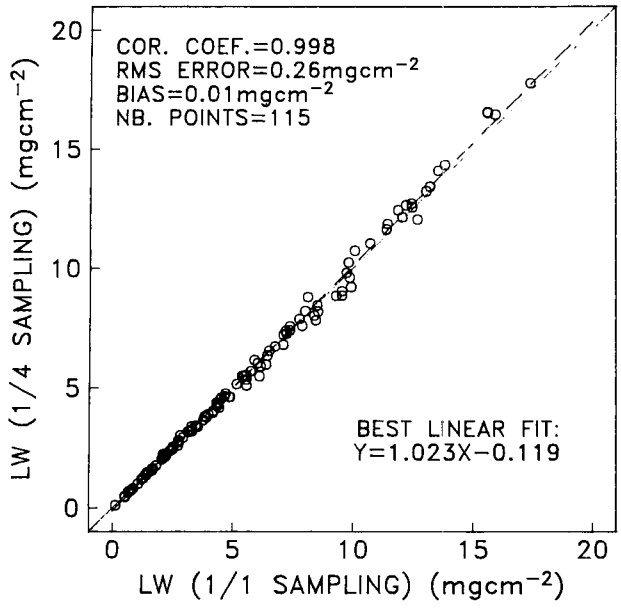

FIG. 4. Spatial sampling effect on VISSR liquid water content estimates.

of interest and over the tropical oceans in general. The results displayed in Fig. 4 indicate a rms difference (after best linear fit) of 0.26 mg cm^{-2} between the two types of estimates. The bias, as expected, is negligible. In June and July, unfortunately, stratocumulus clouds usually occur off southern California, and 60 × 60 km areas containing liquid water contents above 20 mg cm^{-2} could not be found. In this respect, it should be pointed out that differences between the eight VISSR detectors, as well as the lower sensitivity of reflectance to liquid water content above liquid water contents of 20 mg cm^{-2}, may contribute to rms differences larger than 0.26 mg cm^{-2} in the range 20–100 mg cm^{-2}.

Figure 5 shows SMMR and VISSR liquid water content images for 17 June 1979, obtained by applying the above procedure. Examining these images, except for the advection correction (not applied in this picture), one notices that the major features in the SMMR and corresponding VISSR images are similar. The validity of the comparison is more clearly depicted in the scatter plot of Fig. 6, in which the comparison statistics are given (all days were included in the calculations and the advection correction applied). The data were smoothed (over 3 × 3 pixels) by a uniform filter to minimize variability effects. Although the correlation coefficient is high (0.829), the bias between the two types of estimates is large (24.5 mg cm^{-2}).

4. Improved algorithms

Using the VISSR-derived liquid water content as a reference, it is possible to develop algorithms that provide a better correspondence between liquid water content and SMMR brightness temperature.

The quantity LW is first expressed as a linear combination of the logarithm of the difference between T_e (280 K) and the actual T_B in the 18, 21, and 37 GHz channels. In that case, the regression is performed in two ways: 1) by keeping T_e constant (280 K) for each channel (this assumes that the Wilheit and Chang regression coefficients do not correspond to reality); 2) by keeping the Wilheit and Chang coefficients, but considering the equivalent temperature as a variable (this assumes that the brightness temperatures are biased). The general form of the linear combinations are:

1) multilinear regression:

$$\mathrm{LW} = \alpha_0 + \sum_{k=1}^{6} \alpha_k \log_e(280 - T_{Bk}) \qquad (11)$$

2) temperature bias adjustment:

$$\mathrm{LW} = \alpha_0 + \sum_{k=1}^{6} \alpha_k \log_e(T_{ek} - T_{Bk}) \qquad (12)$$

where T_{Bk} is the brightness temperature in channel k (k = 1, 6 for channel 18H, 18V, 21H, 21V, 37H, and 37V, respectively) and T_{ek} is the equivalent temperature in channel k. (H denotes horizontal polarization and V vertical polarization.) In (11) the parameters to be determined are α_0 and α_k, and in (12), T_{ek}.

Another way to account for nonlinearities in the theoretical relationship between brightness temperatures and liquid water content, as well as the correlation between brightness temperatures in different channels (due, for instance, to surface and polarization effects) is to perform a polynomial regression on the brightness temperatures. Therefore LW is written as a second order polynomial with 28 coefficients:

$$\mathrm{LW} = \alpha_0 + \sum_{k=1}^{6} \alpha_{0j} T_{Bj} + \sum_{i=1}^{6} \sum_{j=1}^{6} \alpha_{ij} T_{Bi} T_{Bj} . \qquad (13)$$

For each of the new algorithms, the regression is performed using the June 11, 21, 23, and 29 pairs of SMMR and VISSR images and the results are then verified using the remaining pair of images (those of 17 June. For the algorithm defined by (11), it was not considered necessary to take into account the satellite zenith angle, since this angle (θ) was constant to within ±0.16° (the θ variations would be more consequential for other parameters such as wind speed).

Tables 2, 3, and 4 give the various regression coefficients. The regression statistics on the 1161 points of the selected images (all except those of 17 June) indicate rms differences (after regression) of 7.0, 4.9, and 4.3 mg cm^{-2} for the temperature bias adjustment, the multilinear regression, and the polynomial development, respectively. The α_k in Table 2, which corresponds to the multilinear regression algorithm, are substantially different from those of the Wilheit and Chang algorithm [see Eq. (4)]. Shifting the liquid water content given by Eq. (4) (i.e., modifying α_0) is not sufficient to provide the best regression statistics. The weight of the 37H GHz channel, in particular, has to be decreased by a factor of about 5.

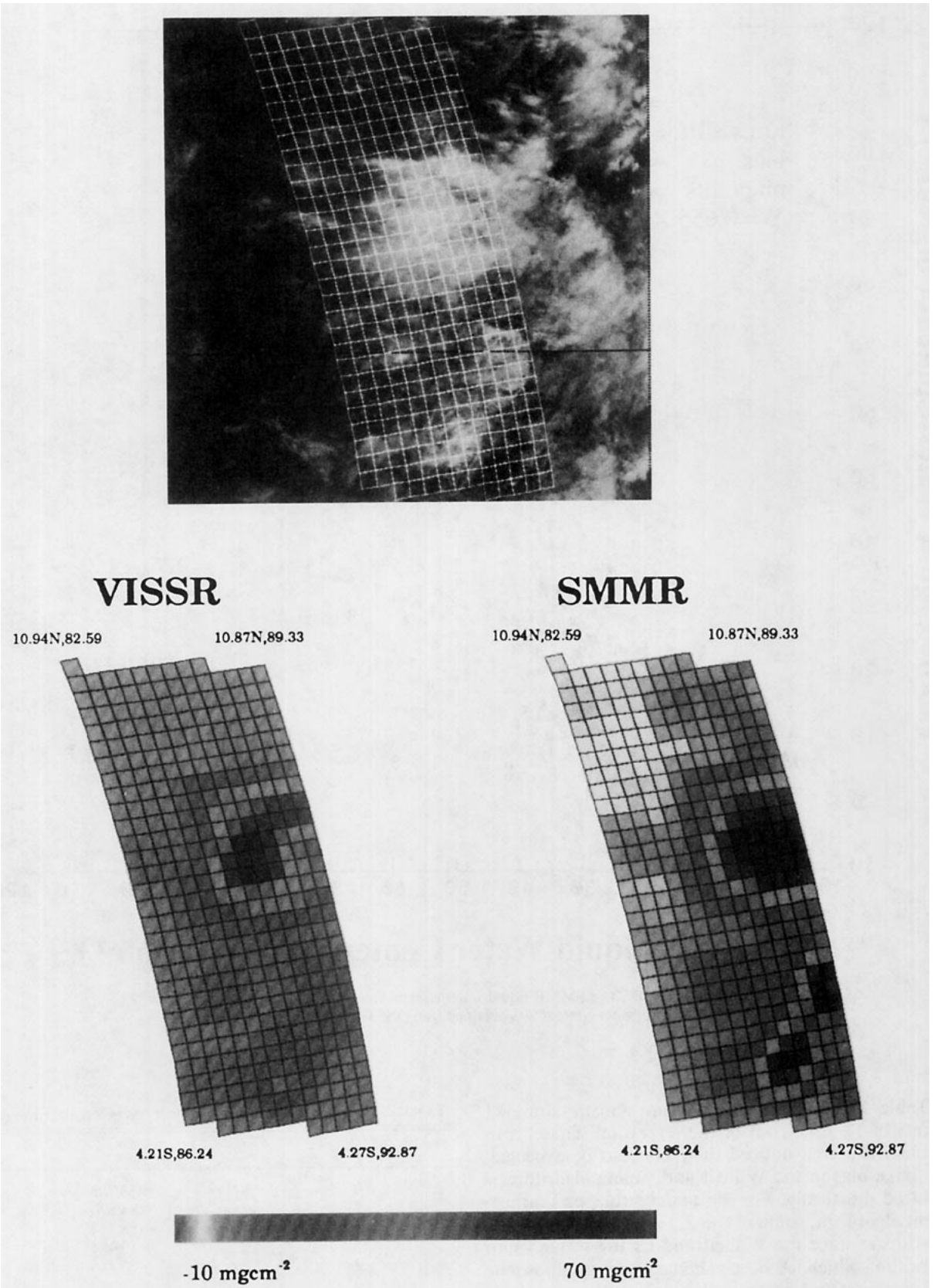

FIG. 5. Liquid water content images obtained from SMMR brightness temperatures (using the Wilheit and Chang algorithm) and VISSR radiance measurements in the visible (using the Stephens et al. 1984 model) over the Indian Ocean on 17 June 1979. Each grid box is 60 × 60 km in size.

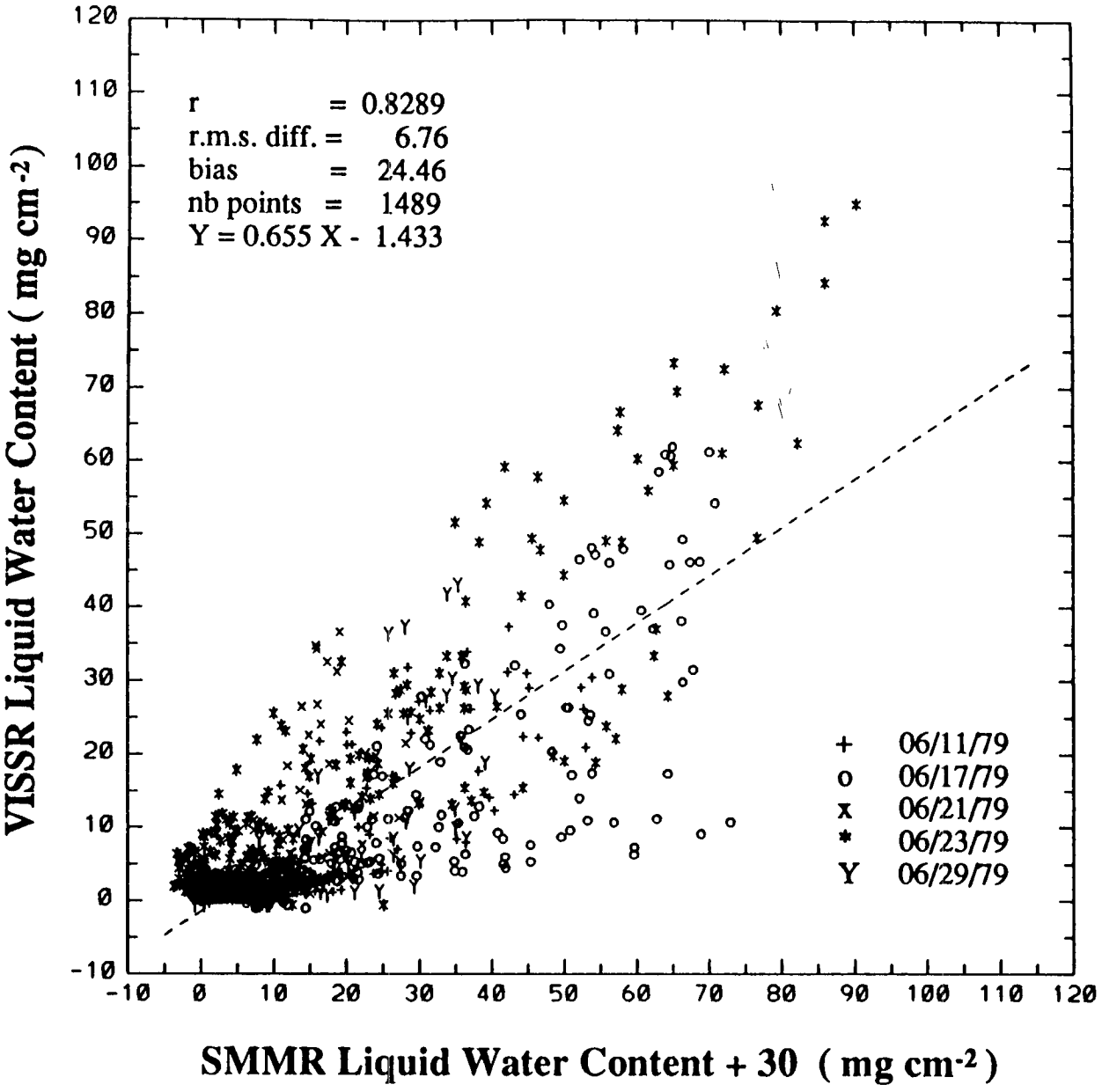

FIG. 6. Scatter plot of VISSR vs SMMR liquid water content for 11, 17, 21, 23, and 29 June 1979. The SMMR liquid water content was obtained using the Wilheit and Chang algorithm.

Table 5 shows the comparison statistics for 341 points of 17 June (out of the regression dataset). In Table 5 it is first noticed, as could be expected, the large bias in the Wilheit and Chang algorithm is reduced drastically. For the temperature bias adjustment algorithm, some of the T_{ek} values in Table 3 are unrealistic since the Wilheit and Chang water vapor algorithm, which has been validated against radiosonde observations and employs the same frequency channels, works well with a T_e value of 280 K. Although the comparison statistics are good for the polynomial

TABLE 2. Coefficients* for the multilinear regression algorithm.

k	α_k
0	456.708
1	84.820
2	−186.114
3	10.484
4	35.486
5	−20.410
6	−28.235

* give LW in mg cm^{-2}

TABLE 3. Coefficients* and equivalent temperatures for the temperature bias adjustment algorithm.

k	α_k	T_{ek}
0	246.1–3.391θ	—
1	134.4	318
2	−51.72	255
3	24.95	289
4	46.14	319
5	−36.63	286
6	−155.5	305

* give LW in mg cm^{-2}

development, the correlation coefficient is significantly lower than that obtained for the multilinear development (0.843 instead of 0.910).

Figure 7 shows the result obtained with the multilinear regression algorithm on the 17 June pair of images. This figure is to be compared with Fig. 6, where for this particular day (represented by the open circles), the correlation between VISSR and SMMR estimates was low.

5. Discussion and concluding remarks

The study has shown that a strong correlation exists between liquid water content derived from SMMR brightness temperatures and VISSR radiances in the visible. This correlation, although established from a limited dataset, allowed the study to adjust the regression coefficients in the Wilheit and Chang algorithm. Such an adjustment may be needed because the algorithm does not work properly (e.g., yields negative values).

The comparison statistics on the entire dataset indicated a 0.83 correlation coefficient, with a confidence range of variation of 0.81 to 0.85 at the 99 percent confidence level for the Wilheit and Chang algorithm. The two values of the correlation coefficients obtained on 17 June for the temperature bias adjustment and the multilinear regression are outside the confidence interval of the Wilheit and Chang algorithm and are significantly different. For that same day, the rms difference between SMMR and VISSR estimates decreases from 7.1 to 6.1, 5.2, and 6.7 mg cm^{-2} for the temperature bias adjustment, the multilinear regression, and the polynomial development algorithms, respectively, and the biases are much smaller in magnitude, changing from 19.1 to −3.3, −2.9 and −1.9 mg cm^{-2}. The temperature bias adjustment, however, yields unrealistic equivalent temperatures. The polynomial development algorithm appears to be more sensitive to surface conditions.

That the Wilheit and Chang algorithm occasionally gives negative values remains to be explained. Although there is no explanation here, the negative values may result from uncertainties in the radiative transfer model and/or a not fully representative regression dataset. It is noted in this respect that Wilheit and Chang did not consider sea surface temperatures above 299 K whereas sea surface temperatures reached 303 K in the study area during the period of interest (e.g., Molinari et al. 1986). It is also possible, due to uncertainties in the surface emissivity model, that sea state effects are not eliminated properly. The above sources of error, however, are unlikely to produce negative values because the algorithm works properly for water vapor content (e.g., Gloersen et al. 1984). On the other hand, the effect of precipitating clouds, not accounted for in the Wilheit and Chang algorithm, is to increase the liquid water content estimates (leading to a positive bias). Still, the possibility remains that the 37 GHz channels are biased (these channels are not used in the water vapor algorithm); but the results of the temperature bias adjustment suggest the opposite.

It should be emphasized that the data analyzed here, namely five pairs of concurrent SMMR and VISSR liquid water content images over the Indian Ocean in June 1979, do not represent worldwide conditions. Furthermore, the VISSR-derived liquid water content is taken as a reference, but the theoretical relationship between cloud albedo and liquid water content applied in the retrieval scheme requires more verification. In addition, cloud albedo in the visible is not sensitive to variations in liquid water content higher than 100 mg cm^{-2}. Using the improved algorithms above this value, therefore, is not warranted. Here the study reminds that Wilheit and Chang only used liquid water contents less that 80 mg cm^{-2} in their simulations. Consequently, their algorithm may also not be applicable above this value.

TABLE 4. Coefficients* for the polynomial development algorithm.

		j						
	α_{ij}	0	1	2	3	4	5	6
	0	2523.939	26.305	−83.538	−5.099	47.978	2.894	−16.828
	1		0.474	−1.065	0.108	0.149	−0.591	0.399
	2			0.307	0.114	−0.179	0.476	0.245
i	3				−0.108	0.125	−1.687E-3	−6.747E-2
	4					−6.316E-2	2.637E-2	−0.176
	5						0.227	−0.435
	6							0.107

* give LW in mg cm^{-2}

TABLE 5. Statistics of comparisons between SMMR and VISSR liquid water content for 17 June 1979.

SMMR Algorithm	Number of points	Correlation coefficient	Rms difference (mg cm^{-2})	Bias (mg cm^{-2})
Wilheit and Chang (1979)	341	0.823	7.0	19.1
Temperature Bias Adjustment	341	0.873	6.0	−3.3
Multilinear Regression	341	0.910	5.0	−2.9
Polynomial Development	341	0.843	6.0	−1.9

Compared to visible techniques, microwave techniques have definitely the advantage of being sensitive to liquid water contents larger than 100 mg cm^{-2}. The spatial resolution of satellite-borne microwave instruments, however, is coarse (typically 30 km at 37 GHz), and for radiative transfer problems, particularly for calculating atmospheric heating rates, it is important to know the spatial distribution of liquid water within

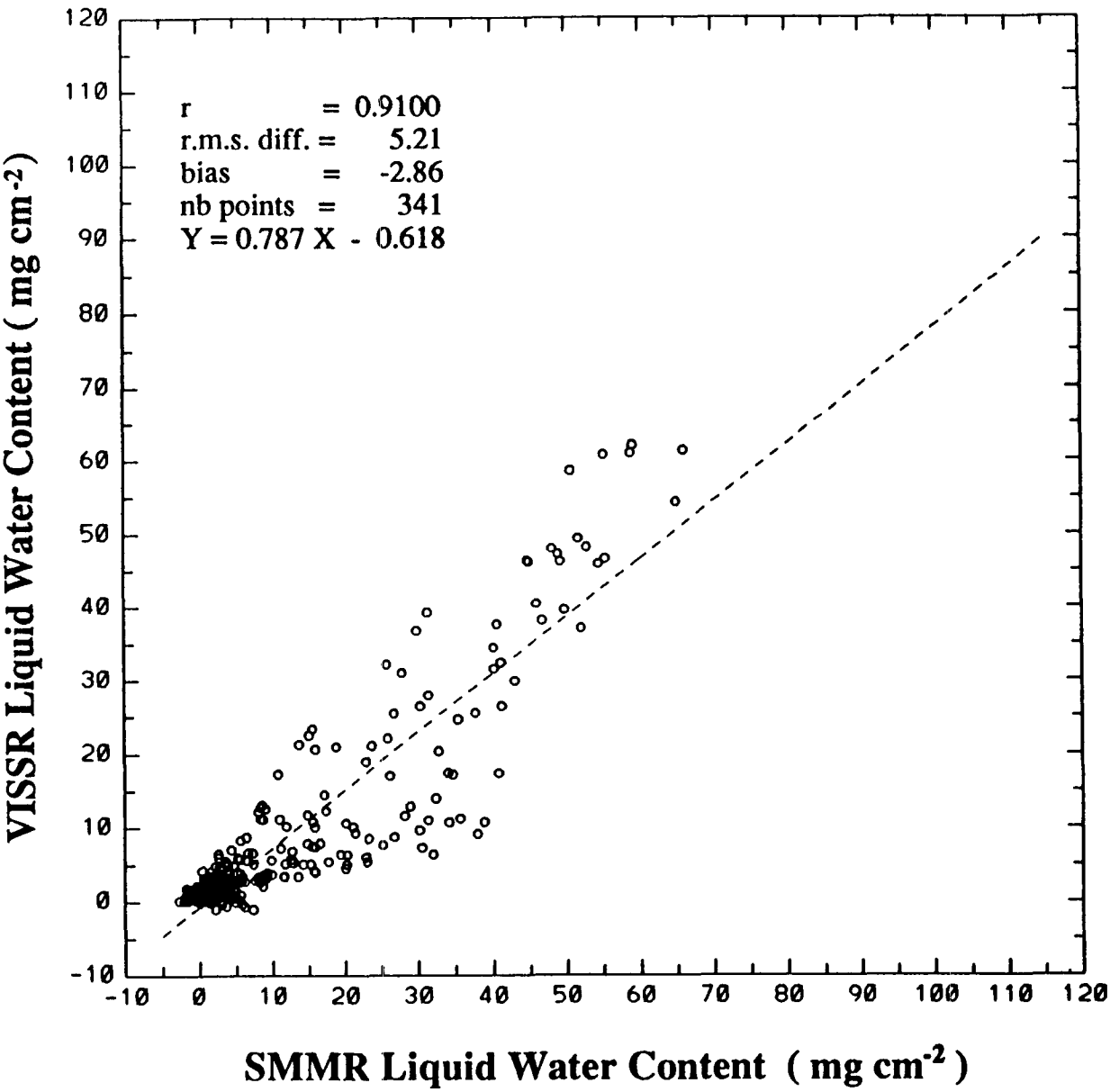

FIG. 7. Scatter plot of VISSR vs SMMR liquid content for 17 June 1979. The SMMR liquid water content was obtained using the multilinear regression algorithm.

such a distance. On the other hand, microwave techniques are sensitive to rain, which makes them inaccurate in the case of precipitating clouds. Regarding visible techniques, the advantage is spatial resolution (and temporal resolution when the sensor is aboard a geostationary satellite), but the techniques are not applicable at night and are limited to liquid water contents lower than 100 mg cm^{-2}. In addition, the presence of cirrus or ice in clouds may bias the liquid water content estimates.

Even though the limitations of the present study are fully recognized which, in particular, needs to be extended to other cloud cases, the results provide useful information on a basic liquid water algorithm. It appears that the main problem with the Wilheit and Chang algorithm is not simply a bias as suggested by Katsaros and Lewis (1986). Designing an accurate liquid water content algorithm for SMMR or other earth-orbiting microwave sensors, in particular the Special Sensor Microwave/Imager (SSM/I), necessitates not only theoretical simulations, which are indeed essential, but also comparisons of the type presented here since validation against actual liquid water contents (in situ measured) is extremely difficult, if not virtually impossible owing to the difficulty of making liquid water content measurements, the spatial variability of liquid water content, and the size of the microwave pixels.

An interesting aspect of the present study for possible future research concerns estimating insolation over the oceans. The proposed algorithms give more accurate access to cloud transmittance in the solar spectrum, a strong function of liquid water content. This transmittance is one of the two major parameters governing insolation variability at the ocean surface, the other one being the sun zenith angle. If problems associated with liquid water distribution within an SMMR pixel can be solved, perhaps statistically, it may then become possible to estimate surface insolation over the global oceans from SMMR, or other microwave radiometer (e.g., SSM/I) data alone. Insolation can indeed be obtained from other datasets, most notably from geostationary satellite observations (e.g., Gautier et al. 1980) Pinker and Ewing 1985; Dedieu et al. 1987), and these observations are available on better spatial and temporal scales, but the microwave approach remains interesting because the latent heat flux across the ocean–atmosphere interface can be estimated with a reasonable accuracy from SMMR data (e.g., Liu 1988). Therefore, from SMMR data alone, the two major components of the ocean surface heat budget would be obtained.

Acknowledgments. Support for this work has been provided by the Centre National de la Recherche Scientifique, France, the Centre National d'Etudes Spatiales, France, and the California Space Institute, Scripps Institution of Oceanography, San Diego. The authors wish to thank Catherine Gautier for providing helpful comments during the study and for making available the VISSR and SMMR datasets; Francois-Marie Bréon for constructive criticisms on some aspects of the manuscript; Beth DiJulio and Jude Correa for technical assistance; and Brian Bloomfield for editing suggestions.

With great admiration and esteem we remember our colleague René Bernard, who passed away on 5 February 1990.

REFERENCES

Coakley, J. A. Jr., and P. Chylek, 1975: The two-stream approximation in radiative transfer: including the angle of the incident radiation. *J. Atmos. Sci.*, **32,** 409–418.

—— and J. B. Snider, 1989: Observed reflectivities and liquid water content for marine stratocumulus. *Proc. Symposium on the Role of Clouds in Atmospheric Chemistry and Global Climate,* Amer. Meteor. Soc., 175–177.

Davis, J. M., and S. K. Cox, 1981: Regional properties of angular reflectance models. *Atmos. Sci. Pap.*, **338,** Colorado State University, 196 pp.

Dedieu, G. P., Y. Deschamps and Y. H. Kerr, 1987: Satellite estimation of solar irradiance at the surface of the earth and of surface albedo using a physical model applied to Meteosat data. *J. Climate Appl. Meteor.* **26,** 79–87.

Diak, G. R., and C. Gautier, 1983: Improvements to a simple physical model for estimating insolation from GOES data. *J. Climate Appl. Meteor.*, **22,** 505–508.

Fairall, C. W., J. E. Hare and J. B. Snider, 1989: An eight month climatology of marine stratocumulus cloud fraction, albedo, and integrated liquid water. *Proc., FIRE science meeting,* Monterey, California, 39–43.

Foot, J. S., 1988: Some observations of the optical properties of clouds, I: Stratocumulus. *Quart. J. Roy. Meteor. Soc.*, **144,** 129–144.

Fu, C. C., 1985: User's guide for the Nimbus-7 Scanning Multichannel Microwave Radiometer (SMMR) CELL-ALL Tape. NASA GSFC Doc. SASC-T-5-5100-0004-011-84,

Gautier, C., G. Diak, and S. Masse, 1980: A simple physical model to estimate incident solar radiation at the surface from GOES satellite data. *J. Appl. Meteor.*, **19,** 1005–1012.

Gloersen, P., D. J. Cavalieri, A. T. C. Chang, T. T. Wilheit, W. J. Campbell, O. M. Johannessen, K. B. Katsaros, K. F. Kunzi, D. R. Ross, D. Staelin, E. R. L. Windsor, F. T. Barath, P. Gudmandsen and E. Langham 1984: A summary of results from the first NIMBUS-7 SMMR observations. *J. Geophys. Res.*, **89,** 5335–5344.

Hignett, O., 1987: A study of the shortwave radiative properties of marine stratus: aircraft measurements and model calculations. *Quart. J. Roy. Meteor. Soc.*, **113,** 1011–1024.

Katsaros, K. B., and R. M. Lewis, 1986: Mesoscale and synoptic-scale features of north Pacific weather systems observed with the scanning multichannel microwave radiometer on NIMBUS-7. *J. Geophys. Res.*, **91,** 2321–2330.

Liu, W. T., 1988: Moisture and latent heat flux variabilities in the tropical Pacific derived from satellite data. *J. Geophys. Res.*, **93,** 6749–6760.

Millet, J. M., 1984: Détermination du contenu en eau de l'atmosphère par radiométrie hyperfréquence spatiale. Ph.D. thesis, Université de Paris VII,

Pinker, R. T., and J. A. Ewing, 1985: Modeling surface solar radiation: model formulation and validation. *J. Clim. and Appl. Meteor.*, **24,** 389–401.

Molinari, R. L., J. F. Festa and E. Marmolejo, 1986: Heat budget and climatic atlas of the tropical western Indian Ocean and Arabian Sea during FGGE. 1979. NOAA Technical Memo ERL AOML-63, 76 pp.

Prabhakara, C., I. Wang, A. T. C. Chang and P. Gloersen, 1983: A statistical examination of NIMBUS-7 SMMR data and remote sensing of sea surface temperature, liquid water content in the

atmosphere, and surface wind speed. *J. Climate Appl. Meteor.*, **22,** 2023–2037.

Smith, W. L., L. D. Herman, T. E. Schreiner, H. B. Howell and P. Menzel, 1980: Radiation budget characteristics of the onset of the summer monsoon. reprints, *Int. Conf. on Early Results of FGGE and Large-Scale Aspects of its Monsoon Experiment,* Tallahassee, FL, 11 pp.

Stephens, G. L., 1978a: Radiation profiles in extended water clouds. Part I: Theory. *J. Atmos. Sci.,* **35,** 2111–2122.

——, 1978b: Radiation profiles in extended water clouds. Part II: Parameterization schemes. *J. Atmos. Sci.,* **35,** 2123–2132.

——, G. W. Paltridge and C. M. R. Platt, 1978: Radiation profiles in extended water vapor clouds. Part III: Observations. *J. Atmos. Sci.,* **35,** 2133–3141.

——, S. Ackerman and E. A. Smith, 1984: A shortwave parameterization revised to improve cloud absorption. *J. Atmos. Sci.,* **41,** 687–690.

Taylor, P. K., T. H. Guymer, K. B. Katsaros and R. G. Lipes, 1983: Atmospheric water distributions determined by the SEASAT Multichannel Microwave Radiometer. *Variations of the Global Water Budget,* A. Street-Perrot, M. Beran and R. Ratcliffe, eds., O. Reidel, 93–106.

Taylor, V. R., and L. Stowe, 1984: Reflectance characteristics of uniform earth and cloud surfaces derived from Nimbus-7 ERB. *J. Geophys. Res.,* **89,** 4987–4996.

Teillet, P. M., P. N. Slater, Y. Mao, Y. Ding, Y. Yuan, R. J. Bartell, S. F. Biggar, R. P. Santer, R. D. Jackson and M. S. Moran, 1988: Absolute radiometric calibration of the NOAA AVHRR sensors. *Proc. SPIE,* 23–27.

Welch, R. M., S. K. Cox and J. M. Davis, 1980: Solar radiation and clouds. Amer. Meteor. Soc., 96 pp.

Whitlock, C. H., W. F. Staylor, G. Smith, R. Levin, R. Frouin, C. Gautier, P. M. Teillet, P. N. Slater, J. Y. Kaufman, B. N. Holben and S. R. LeCroy, 1990: AVHRR and VISSR satellite instrument calibration results from both cirrus and marine stratocumulus IFO periods. NASA CP-3083, in press.

Wilheit, T. T., and A. T. C. Chang, 1979: An algorithm for retrieval of ocean surface and atmospheric parameters from the observations of the Scanning Multichannel Microwave Radiometer (SMMR). NASA/GSFC Tech. Memo. 80277, 41 pp.